Quantitative Rectangular Notch Detection of Laser-induced Lamb Waves in Aluminium Plates with Wavenumber Analysis

Liu Zenghua[1,2*], *Feng Xuejian*[1,2], *He Cunfu*[1,2], *Wu Bin*[1,2]

1. College of Mechanical Engineering and Applied Electronics Technology, Beijing University of Technology, Beijing 100124, P. R. China;
2. Beijing Engineering Research Center of Precision Measurement Technology and Instruments, Beijing University of Technology, Beijing 100124, P. R. China)

(Received 23 December 2017; revised 2 March 2018; accepted 28 March 2018)

Abstract: It is difficult to quantitatively detect defects by using the time domain or frequency domain features of Lamb wave signals due to their dispersion and multimodal characteristics. Therefore, it is important to discover an intrinsical parameter of Lamb waves that could be used as a damage sensitive feature. In this paper, quantitative defect detection in aluminium plates is carried out by means of wavenumber analysis approach. The wavenumber of excited Lamb wave mode is a fixed value, given a frequency, a thickness and material properties of the target plate. When Lamb waves propagate to the structural discontinuity, new wavenumber components are created by abrupt wavefield change. The new wavenumber components can be identified in the frequency-wavenumber domain. To estimate spatially dependent wavenumber values, a short-space two-dimensional Fourier transform(FT) method is presented for processing wavefield data of Lamb waves. The results can be used to determine the location, size and depth of rectangular notch. The analysis techniques are demonstrated using simulation examples of an aluminium plate with a rectangular notch. Then, the wavenumber analysis method is applied to simulation data that are obtained through a range of notch depths and widths. The results are analyzed and rules of the technique with regards to estimating notch depth are determined. Based on simulation results, guidelines for using the technique are developed. Finally, experimental wavefield data are obtained in aluminium plates with rectangular notches by a full non-contact transceiving method, i. e., laser-laser method. Band-pass filtering combined with continuous wavelet transform is used to extract a certain frequency component from the full laser-induced wavefield with wide band. Short-space two-dimensional FT method is used for further processing full wavefield data at a certain frequency to estimate spatially dependent wavenumber values. The consistency of simulation and experimental results shows the effectiveness of proposed wavenumber method for quantitative rectangular notch detection.

Key words: wavenumber analysis; short-space two-dimensional Fourier transform(FT); notch; aluminium plate

CLC number: TG156 **Document code**: A **Article ID**: 1005-1120(2018)02-0244-12

0 Introduction

Notch is one of the most common defect types in aluminium aircraft structures. Lamb waves have shown great potential for non-destructive testing and structural health monitoring purposes in plate-like structures due to their ability to propagate long distances with low energy loss and their reasonable sensitivity for defects of different types[1-4]. Defect detection technology based on Lamb waves can effectively identify and locate defects by using transducer array, but there are still many challenges in the quantitative detection of defects[5]. The recent progresses on wavefield analysis technique have provided a new way to achieve quantitative detection of defects[6-7]. Some scholars have also proposed the phased array imaging method for defects detection

* Corresponding author, E-mail address: liuzenghua@bjut.edu.cn.

How to cite this article: Liu Zenghua, Feng Xuejian, He Cunfu, et al. Quantitative rectangular notch detection of laser-induced Lamb waves in aluminium plates with wavenumber analysis[J]. Trans. Nanjing Univ. Aero. Astro., 2018,35(2): 244-255.

http://dx.doi.org/10.16356/j.1005-1120.2018.02.244

and location in plates, as well as the wavefield analysis and other techniques for defect quantification[8-9]. Recently, with the development of laser ultrasonic technology, ultrasonic optical testing equipment, represented by laser Dopper vibrometer and two-wave mixing interferometer, has been widely used in the wavefield measurement. The two-wave mixing interferometer provides a high spatial resolution measurement of the out-of-plane displacement component at both one-dimensional (1D) and two-dimensional (2D) spaces, and wavefield signal is further analyzed by multi-dimensional Fourier transform(FT) to reveal the characterization of the defect[10]. In the existing wavefield analysis based on multi-dimensional FT, the wavenumber analysis exhibits great potential in the quantitative detection of defects[11-16].

This paper illustrates the process of the wavenumber analysis to realize the quantitative detection of the rectanguar notch depth, and provides a feasible non-contact quantitative defect detection method. Firstly, the simulation models of different notches with different depths and widths are established to obtain the effects of notch depth, notch width and window width on the quantitative detection accuracy of wavenumbr analysis. Then, the finite element analysis is performed on experimental plates and the simulated data are analyzed by wavenumber analysis. Further, the experimental system is establised, and the aluminum plate with different notch depths are quantitatively detected. In the experiment, the Nd:YGA pulsed laser is used as the actuator of Lamb waves, and the signal is obtained by two-wave mixing interferometer. Finally, the results of experiment and simulation verify the effectiveness of wavenumber and analysis method.

1 Wavenumber Analysis

Wavenumber is one of the intrinsical parameters of Lamb waves. The wavenumber of excited Lamb wave mode is a fixed value for a given frequency, a given thickness and material properties of the plate. Thus, for the determined excitation frequency and plate properties, the corresponding plate thickness can be calculated according to wavenumber. The defects in plate-like structure will cause the thickness of the plate change. Therefore, the depth of the defect can be quantitatively evaluated according to the wavenumber corresponding to the defect area.

1.1 Lamb wave dispersion characteristics

Lamb waves are dispersive and multi-modal. From Rayleigh-Lamb equation, the relationship between frequency and wavenumber can be calculated in plates. Fig. 1 depicts Lamb waves dispersion curves of a 2 mm-thick aluminium plate. As shown in Figs. 1(a, b), when the values of frequency-thickness product is lower than 1.5 MHz·mm, only the fundamental Lamb waves modes, A_0 and S_0 modes, exist. As the product of frequency and thickness increases, more Lamb wave modes (such as A_1, A_2, S_1, and S_2) appear.

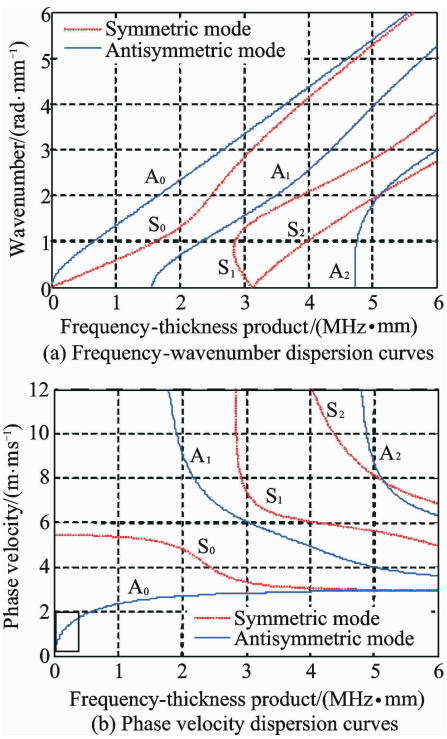

Fig. 1 Lamb waves dispersion curves of a 2 mm-thick aluminium plate

The dispersion characteristics can be represented by Fig. 1(b) for aluminium plate with different thicknesses. Compared with the S_0 mode, the phase velocity of the A_0 mode changes more greatly with plate thickness duo to its highly dis-

persive nature at low frequency-thickness product (fd). Thicker plates will cause greater product of frequency and thickness for a given frequency f, which will cause greater phase velocity eventually. According to the equation $k=2\pi f/v_p$, greater phase velocity v_p results in smaller wavenumber k. Thinner plates will cause greater wavenumber conversely. Therefore, the A_0 mode at low frequency is selected to evaluate the thickness of aluminium plate for the detection of defect depth.

1.2 Two-dimensional Fourier transform

M measured points are taken with a spatial resolution of Δx, and the number of samples per point is N, thus a spatial-temporal data matrix $\boldsymbol{u}(x,t)$ with dimension of $M\times N$ can be obtained. The concept of Fourier analysis is straightforwardly extended to multi-dimensional signals, such as the spatial-temporal wavefield data $\boldsymbol{u}(x,t)$. The frequency-wavenumber representation of a spatial-temporal signal can be interpreted as an alternative representation of the signal in terms of the familiar temporal frequency variable ω and the wavenumber k. For 1D wave propagation, its representation in frequency-wavenumber domain is obtained by 2D FT. Spatial-temporal signal $\boldsymbol{u}(x,t)$ can be transformed to frequency-wavenumber domain by using 2D FT, which is defined as

$$U(k,\omega)=\int_{-\infty}^{+\infty}\int_{-\infty}^{+\infty}\boldsymbol{u}(x,t)\exp^{-\mathrm{j}(\omega t-kx)}\mathrm{d}x\mathrm{d}t \quad (1)$$

where x is the distance between a actuator and a receiver, t the time variable, ω the frequency variable, and k the wavenumber. According to Eq. (1), the amplitude distribution of frequency-wavenumber spectrum depends on wavenumber component contained in wavefield $\boldsymbol{u}(x,t)$ at an interested frequency ω_0. From the dispersion characteristics of Lamb waves, it can be found that the change of the plate thickness at the defect will produce new wavenumber components, which implies that the amplitude distribution of wavenumber spectrum will change at an interested frequency ω_0 in the frequency-wavenumber domain.

1.3 Space-frequency-wavenumber analysis

The wavefield data is transformed from the time-space domain to the frequency-wavenumber domain through 2D FT which reveals the wave propagation characteristics that can not be clearly seen in the time-space domain. However, this approach cannot retain the space or time information. Therefore, according to the change of wavenumber spectrum distribution at a certain center frequency, only whether there exists a defect in the signal propagation path can be determined, while the specific location of the defect remains unknown. Similar to the idea of the short-time FT using a windowing technique, a short-space 2D FT is adopted in this paper to perform the space-frequency- wavenumber analysis where the spatial information is retained. Mathematically, this process can be expressed as

$$Z(x_i,k,\omega)=\int_{-\infty}^{+\infty}\int_{-\infty}^{+\infty}\boldsymbol{u}(x,t)W^*(x-x_i,t)\exp^{-\mathrm{j}(\omega t-kx)}\mathrm{d}x\mathrm{d}t \quad (2)$$

where x_i is the space index, $W(x,t)$ the 2D window function. If $|x|\leqslant D_x/2$, the function of $W(x,t)$ can be given

$$W(t,x)=0.5\left[1+\cos\left(2\pi\frac{x}{D_x}\right)\right] \quad (3)$$

Otherwise, $W(t,x)=0$. Here, D_x is the window width in space domain. Previous research has shown that the window width should be greater than at least two wave periods in order to accurately represent the spectral peak[17]. The phase velocity of Lamb waves is calculated according to the wavenumber of the defect region, and the frequency-thickness product corresponding to the phase velocity in the theoretical dispersion curves is selected to calculate the thickness of the aluminium plate at the defect region, so as to evaluate the defect depth.

2 Rectangular Notch Simulation

2.1 Simulation methodology

2D simulation has been implemented using the ABAQUS finite element package in this study. An aluminium plate of 2 mm thickness and 1 000 mm length was modelled for obtaining the effects of notch depth, notch width and window

width on the quantitative detection accuracy of wavenumbr analysis. Material properties of the aluminium plate are listed in Table 1.

Table 1 Material properties of the aluminium plate

Density/ ($kg \cdot m^{-3}$)	Young's modulus/Gpa	Poisson's ratio
2 700	71	0.33

A schematic illustration of the simulation model is shown in Fig. 2. A_0 mode was input according to the displacement mode shape of A_0 in the left end of plate. Here, the three-cycle excitation signal modulated by Hanning window at the center frequency of 200 kHz was used. The simulation was solved using a fixed time stepping solver with 1 ns time step and 0.1 mm maximum quadratic element size in order to satisfy the requirements of the stability and accuracy of the solution. Notch was 100 mm away from the left end of the model.

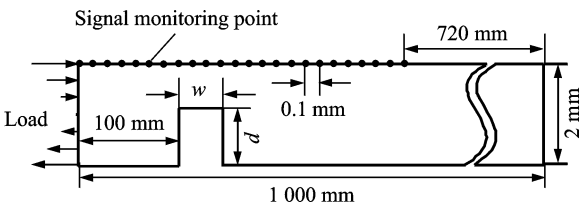

Fig. 2 Schematic illustration of simulation model

2.2 Simulated wavefield analysis

As illustrated in Fig. 2, taking the left end of the model as the starting point, the out-of-plane components were taken from left to right side of the model with a spatial resolution of 1 mm, and 281 points were extracted. Take the defected model as an example, the notch width w is 20 mm and the depth d is 1.5 mm, and the simulation data were analyzed by space-frequency-wavenumber analysis method. A 2D Hanning window with a width of 20 mm (equal to notch width) was selected and the moving step size was 1 mm. The resulted time-space wavefield and its frequency-wavenumber spectrum are shown in Fig. 3(a) and Fig. 3(b), respectively. Fig. 3(a) shows transmitted, reflected and multiple reflected waves caused by notch, as well as the incident wave. Furthermore, when the signal propagates inside the notch, the wave velocity decreases (the slope of the incident waves decreases in the distance-time coordinate system), which is consistent with the propagation characteristics of A_0 mode shown in Fig. 1(b). The frequency-wavenumber spectrum is plotted as amplitude versus frequency and wavenumber in Fig. 3(b), together with the theoretical dispersion curves. As shown in Fig. 3(b), the A_0 mode can be clearly observed, and the simulation results match well with the theoretical dispersion curves. It can be also observed that the new wavenumber component induced by notch matches well with the theoretical dispersion curves of aluminium plate with 0.5 mm thickness. Note that in the frequency-wavenumber spectrum, negative wavenumbers represent waves that propagate opposite to the incident wave.

Fig. 3(c) presents the space-wavenumber spectrum at 200 kHz. As shown in Fig. 3(c), the spectrum corresponding to waves propagating in the defect-free zone is centered about the wavenumber at 0.72 rad/mm, which is the same as the theoretical wavenumber value of A_0 mode at 200 kHz in the pristine region of the model. Furthermore, the spectrum corresponding to multiple reflected waves inside the notch increases distinctly and it is centered about the wavenumber at 1.32 rad/mm, which is the same as the theoretical wavenumber value of A_0 mode at 200 kHz in the defect region of the model. Fig. 3(d) shows space-wavenumber curves plotted by calculating the weighted average of the wavenumber at each location. Therefore, the location of the notch and the wavenumber of the notch region can be determined using the peak coordinates of the space-wavenumber curve.

2.3 Parameters analysis by wavenumber analysis

The analysis procedure outlined in Section 2.3 was applied to simulation data which were obtained through a range of notch depths and widths. Notch width ranged from 3 mm to 13 mm in 1 mm increments with a constant 1.8 mm notch depth. Window width ranged from 8 mm to

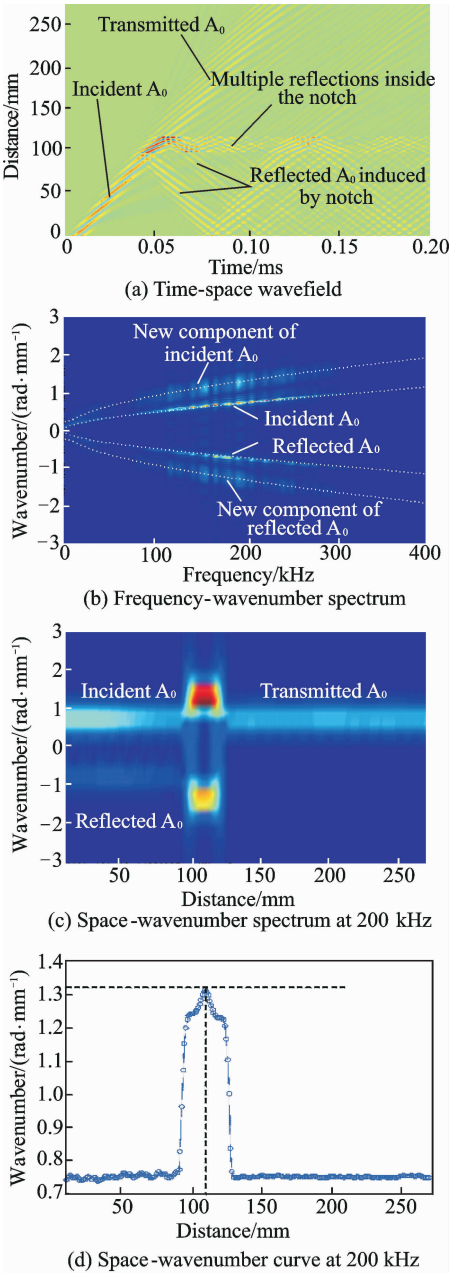

Fig. 3 Space-frequency-wavenumber analysis of simulation data for the model with notch defect

13 mm for each width. The theoretical and calculated wavenumber are shown in Fig. 4(a). The accuracy increases along with the notch width increase. This can be explained by considering that when the notch is smaller than the window, the windowed dataset will contain the signals of Lamb waves propagating within and adjacent to the notch. Therefore, the calculated wavenumber will be reduced by the presence of the lower wavenumber components presented in the pristine region of the plate. Fig. 4(b) shows wavenumber percent error versus the ratio of notch width to window width W_d/W_w. As the notch width increases and approaches the window width, the error is dramatically reduced.

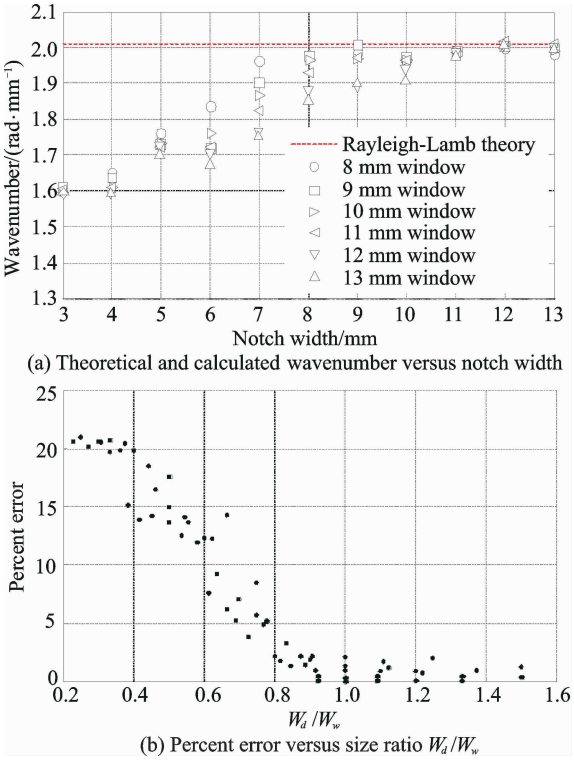

Fig. 4 Effect of notch width on calculated wavenumber at the frequency of 200 kHz and with a 1.8 mm deep notch

Simulations were also performed when notch depth varied from 0.1 mm to 1.8 mm in 0.1 mm increments with constant 30 mm notch width, in order to study the effect of notch depth on calculated wavenumber. Window width ranged from 8 mm to 13 mm. The theoretical wavenumber and calculated wavenumber are shown in Fig. 5(a). Theoretical wavenumber was determined by solving the antisymmetric Rayeigh-Lamb equation at 200 kHz for propagation in a plate with a thickness equal to that of the region inside the notch. Agreement between the theoretical and the calculated wavenumbers was achieved, particularly for the notch depth more than 1.2 mm where maximum percent error is 3.6%. For each notch depth, a larger window results in greater accuracy, particularly for more shallow notch. For the shorter wavelengths corresponding to thinner plate or deeper notch, more cycles of the wave were contained within the window. As shown in

Fig. 5(b), calculated wavenumber percent error is presented versus a normalized window size equal to the product of wavenumber and window width. The normalized window size indicates the number of wavelengths contained in the window. Measurement error is less than 1.7% for normalized window sizes greater than two, which corresponds to two wave periods within the window.

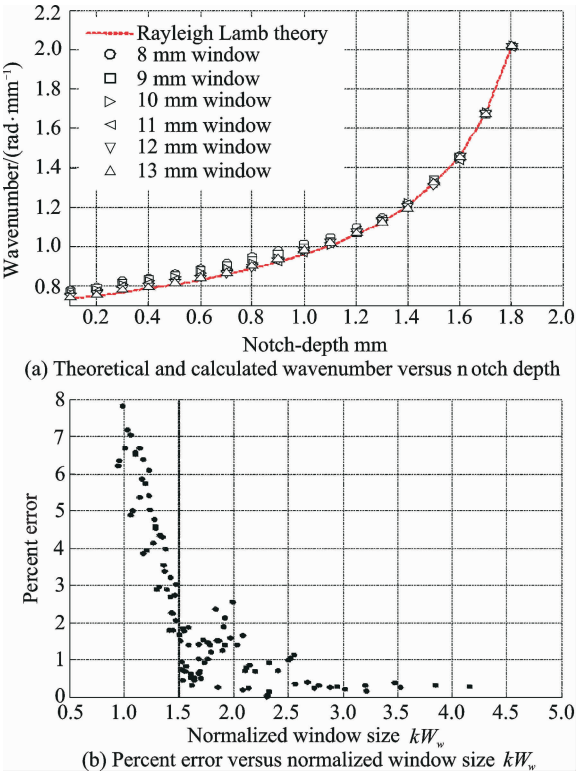

Fig. 5 Effect of notch depth on calculated wavenumber at the frequency of 200 kHz and with a 30 mm notch depth

The simulation results show that when determining the window width, a balance must be struck between increasing window width to ensure multiple wavelengths within the window while reducing window width to ensure the notch width larger than the window width. Therefore, in order to minimize error in wavenumber measurement, the window width must be at least as large as two wavelengths and the notch must be at least as large as the window width.

2.4 Simulation analysis for experimental plate

Using the same modeling method, an aluminium plate of 1.7 mm thickness and 1 000 mm length was modelled. Taking the left end of the model as the starting point, the out-of-plane components were taken from the left to the right side of model with a spatial resolution of 0.5 mm, and 561 points were extracted. The center frequency of excitation signal was 140 kHz, and other simulation parameters remained unchanged. Both pristine and defected simulated data were analyzed using space-frequency-wavenumber analysis. Two notches with different depths were detected: 20 mm × 0.9 mm and 20 mm × 1.4 mm. Hanning window with a width of 20 mm (equal to notch width) was selected and moving step size was 0.5 mm.

Fig. 6 shows analysis results of the pristine plate. As shown in Fig. 6(a), there is only incident signal in the time-space wavefield due to the absence of defects. There is no signal attenuation in the simulation, so it can be seen from Fig. 6(b) that the energy of the signal does not drop clearly as the propagation distance increases. Furthermore, it can be clearly observed from Fig. 6(c) that the wavenumber did not change significantly

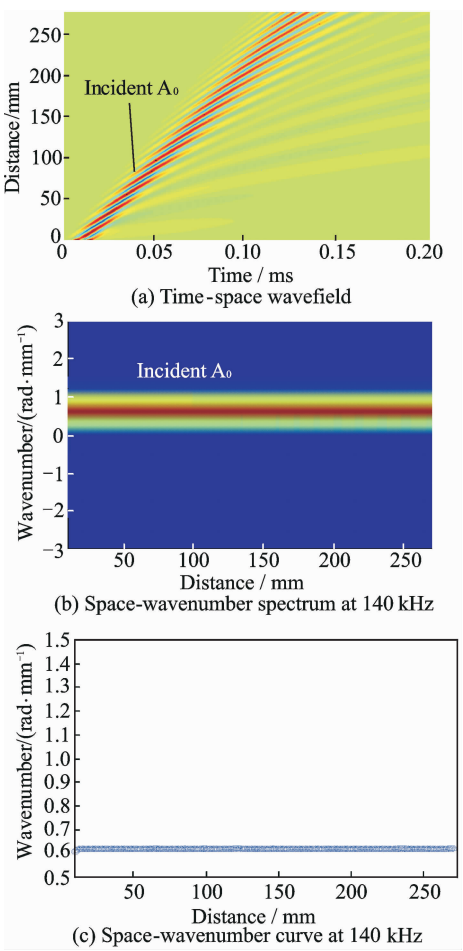

Fig. 6 Space-frequency-wavenumber analysis of simulation data for the pristine model

in the propagation path, and the predicted and calculated wavenumbers well agrees.

Simulated signals obtained from defected models were analyzed, and the results are shown in Figs. 7,8. Compared with the time-space wavefield, it can be seen that transmitted signal components decrease and multiple reflection phenomenon within the notch becomes more obvious as the notch depth increases. Furthermore, as the notch depth increases, the proportion of wavefield energy increases in the defect region as shown in Fig. 7(b) and Fig. 8(b). As the notch depth increases, more portion of Lamb waves are trapped inside the notch due to multiple reflections from the notch boundary, while less Lamb waves are transmitted through notch. As shown in Fig. 7(c) and Fig. 8(c), the wavenumber significantly increases in the defect region. Evaluation results of notch depth obtained from simulation data are listed in Table 2.

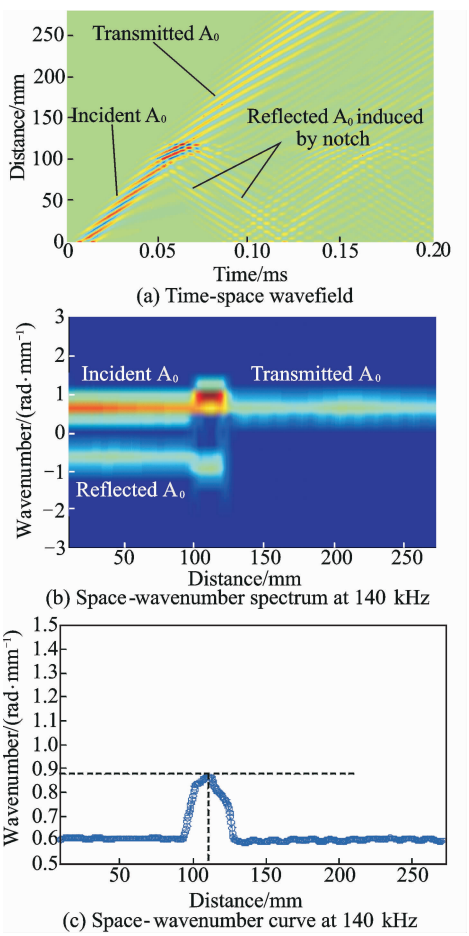

Fig. 7 Space-frequency-wavenumber analysis of simulate data for the model with a 0.9 mm deep notch

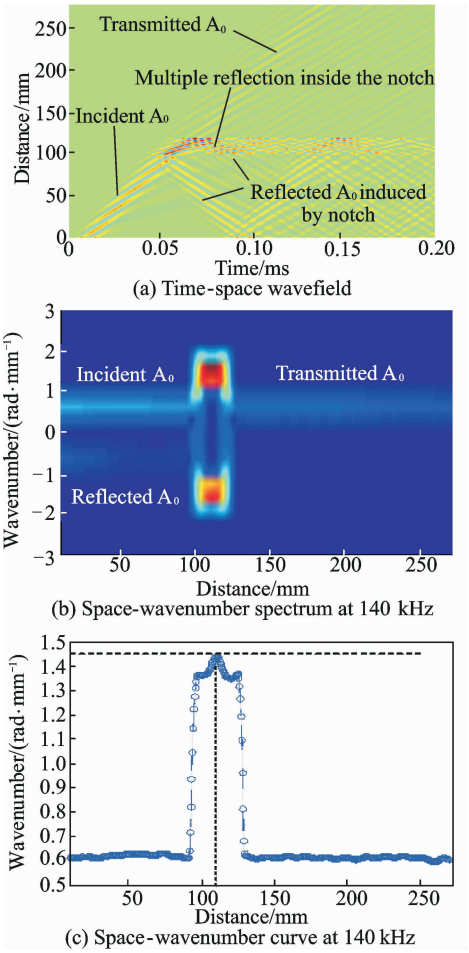

Fig. 8 Space-frequency-wavenumber analysis of simulation data for the model with a 1.4 mm deep notch

Table 2 Evaluation results of notch depth obtained from simulation data

Evaluation result	Notch depth/mm	
	0.9	1.4
Frequency/kHz	140	140
Measured wavenumber/(rad · mm^{-1})	0.86	1.44
Phase velocity/(m · s^{-1})	1 018	610.4
Frequency-thickness product/(kHz · mm)	115.2	40.6
Measured thickness/mm	0.823	0.29
Measured depth/mm	0.877	1.41
Percent error/%	2.5	0.7

3 Experiment

3.1 Test specimens

Three aluminium plates with dimension of 1 000 mm× 1 000 mm×1.7 mm labelled as No. 1, No. 2 and No. 3 were used for testing. No. 1 aluminum plate had no defect. The notch defect

of 30 mm × 20 mm × 0.9 mm was machined on No. 2 aluminium plate and the other notch defect of 30 mm × 20 mm × 1.4 mm was machined on No. 3 aluminium plate . From the back side of the defect, the schematic of the test aluminium plate is shown in Fig. 9. Taking the location of the pulsed laser spot as the origin, a total of 401 scan points along the positive direction of x axis from the $x=0$ mm to 200 mm were taken with a spatial resolution of $\Delta d=0.5$ mm. Note the sampling interval Δd was selected first by meeting the Nyquist sampling theorem spatially, i.e. $\Delta d \leqslant \lambda/2$, where λ is the wavelength of the interrogating wave. To improve the signal-to-noise ratio, the measurement at each scan point was averaged for 30 times. To further improve the measurement quality, reflective tape (producted by 3M corporation, 8850 model, approximately 0.1 mm thick) is used to ensure the consistency of smoothness of the surface of the aluminium plates.

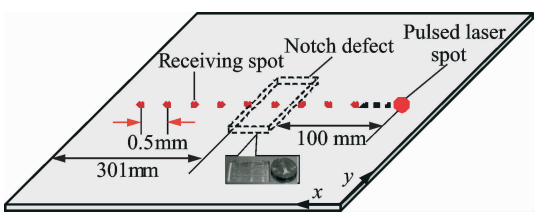

Fig. 9 Schematic of the test aluminium plate

3.2 Experimental setup

The diagram of non-contact laser ultrasonic testing system is shown in Fig. 10. The excitation was implemented by a Nd:YAG pulsed laser. Data acquisition was completed with two-wave mixing interferometer. Then, the data was further collected by a digital oscilloscope (Tektronix DPO 4054B) at a time sampling rate of 50 MHz.

During excitation, the laser controller provided energy for Nd: YAG pulse laser to cause energy transitions in its internal crystal to generate a pulsed laser, which was emitted by the FHY excitation head and acted on the surface of the aluminium plate. At the same time, the laser controller provided the oscilloscope with a synchronous trigger signal to ensure the synchronous excitation and reception of the laser ultrasonic signals.

On the receiving side, the continuous laser was output by a continuous-wave fiber laser, which was split into two beams after passing through the laser splitter drawer. One of them was directly input to the demodulator as a reference light, the other was irradiated to the surface of the aluminium plate via a FHY measurement head, and then the laser (signal light) reflected by the surface of the aluminium plate and carrying the ultrasonic signal received by the FHY measurement head again, and eventually transmitted to the demodulated. In demodulator, the ultrasonic signal was demodulated by reference light and signal light. Finally, it was received and displayed by an oscilloscope. The FHY measurement head was mounted on the 2D control platform, and the position of the meas -

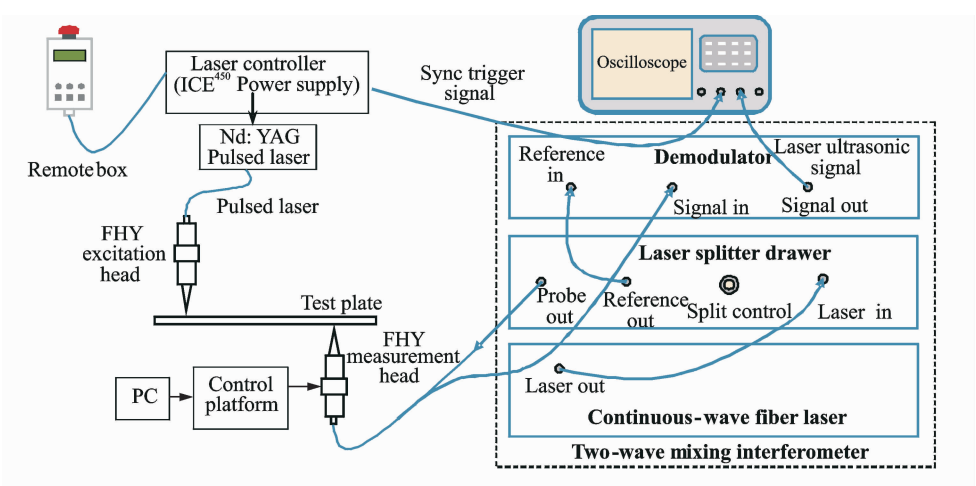

Fig. 10 Diagram of the non-contact laser ultrasonic testing system

urement head can be accurately controlled by the computer. In order to avoid the influence of the air shock wave generated by thermoelastic mechanism on the received signal, the excitation and reception probes were divided into two sides of the aluminium plate.

The wavelength of the laser produced by the Nd: YAG pulse laser in the system was 1 064 nm, the effective duration was 10 ns, the energy of single laser pulse was 0—50 mJ, and the diameter of the spot was about 1.2 mm when the spot was focused. Laser single-pulse energy adjustment and excitation mode selection can be achieved through the laser controller. The laser ultrasonic receiver adopted the AIR-1550-TWM two-wave mixing interferometer produced by the American IOS company. The continuous laser wavelength was 1 550 nm, the spot radius was at least 200 μm, and the detection bandwidth was 125 MHz. In the experiment, in order to ensure that the laser excites the ultrasonic signal under the thermoelastic mechanism to avoid damage to the surface of the aluminium plate, the laser single-pulse energy was set to 10 mJ. To increase the signal-to-noise ratio, the laser excitation and receiving beams were kept perpendicular to the surface of aluminium plate. The experimental system of non-contact laser ultrasonic testing system is shown in Fig. 11.

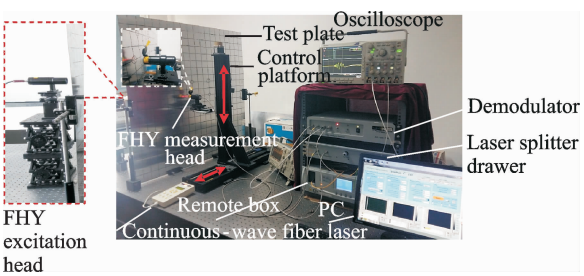

Fig. 11 Experimental system of non-contact laser ultrasonic testing system

3.3 Analysis of received wavefield by laser-laser method

On the basis of band-pass filtering, continuous wavelet transform was used to get wavefield signals with center frequency of 140 kHz. According to the Shannon entropy minimum theory[18] of wavelet coefficients, gaus9 was selected as the mother wavelet. In No. 3 aluminium plate, the time-domain signals of Lamb waves and its frequency spectra received by the receiving spot at 50 mm away from the excitation spot are shown in Fig. 12. As shown in Fig. 12(a), the time-

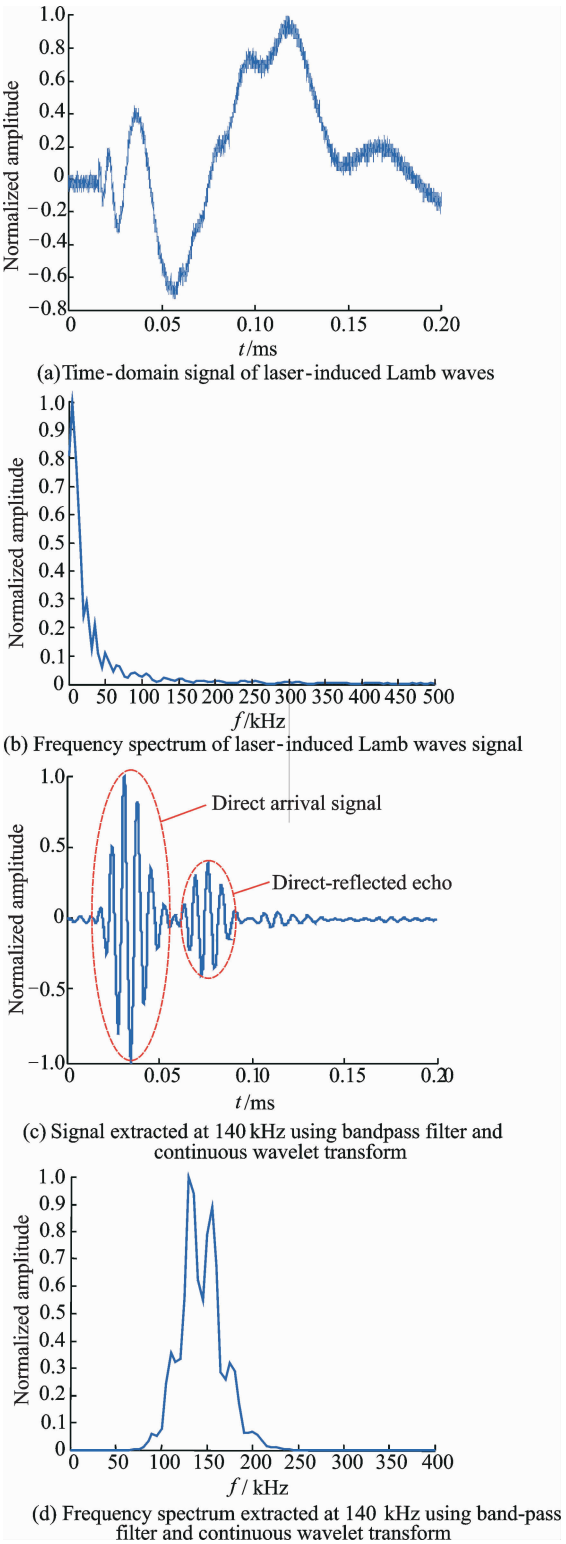

Fig. 12 Time-domain signals and frequency spectra of laser-induced Lamb waves at 50 mm distance from the receiving spot

domain signal of the original laser-induced Lamb waves contain a lot of high-frequency noises, the direct arrival signal and defect-reflected signal can not be clearly seen. However, according to the phenomenon that the amplitude of the signal has many irregular oscillations after 0.05 ms, it can be inferred that after this time point, the signal includes components other than the direct arrival signal. From Fig. 12(b), it can be seen that the laser-induced Lamb wave signal has a wide frequency band and is dominated by low-frequency components, and the energy of high-frequency components is relatively low due to attenuation during the propagation process. After the wavelet denoising of the original laser-induced Lamb wave signal, bandpass filter and continuous wavelet transform were used to extract Lamb wave signal with the center frequency of 140 kHz. The direct arrival signal and the defect-reflected echo can be clearly seen, as Fig. 12(c) shows. The frequency spectrum of the extracted signal as shown in Fig. 12(d), shows that the frequency band of the signal has been concentrated near the center frequency of 140 kHz.

Band-pass filtering combined with continuous wavelet transform was used to extract the wavefield signals of laser-induced Lamb waves collected from the three test plates, and the wavefield signals with the center frequency of 140 kHz were obtained. The analysis results of extracted experimental wavefield are shown in Figs. 13—15. Agreement between the simulated and experimental results is relatively poor. The wavenumber component in the experimental results is more complicated, which has a certain impact on the evaluation of the depth of defects. Evaluation results of notch depth using experimental data obtained by laser-laser method are listed in Table 3. As shown in Table 3, the accuracy of defect depth evaluation in No. 3 test plate is lower than that in No. 2 test plate. The experimental results are not consistent with the conclusions obtained in Section 2.3 and the simulation results in Section 2.4. This is mainly due to the noise contained in the experimental data, which reduces the signal-to-noise ratio. The source of noise mainly comes from the poor consistency of experimental signals. The poor consistency of the experimental signal will affect the quality of the wavefield signal[19], and further affect the accuracy of the final defect depth assessment. The Gauss white noise contained in the experimental data is also one of the factors that reduce the signal-to-noise ratio of the experimental data.

Table 3 Evaluation results of notch depth using experimental data obtained by laser-laser method

Notch depth/mm	Frequency/mm	Measured wavenumber/rad·mm	Phase velocity/(m·s^{-1})	Frequency-thickness product/(kHz·mm)	Measured thickness/mm	Measured depth/mm	Error/%
0.9	140	0.84	1050	120	0.857	0.843	6.3
1.4	140	1.15	788.6	68.1	0.490	1.210	13.6

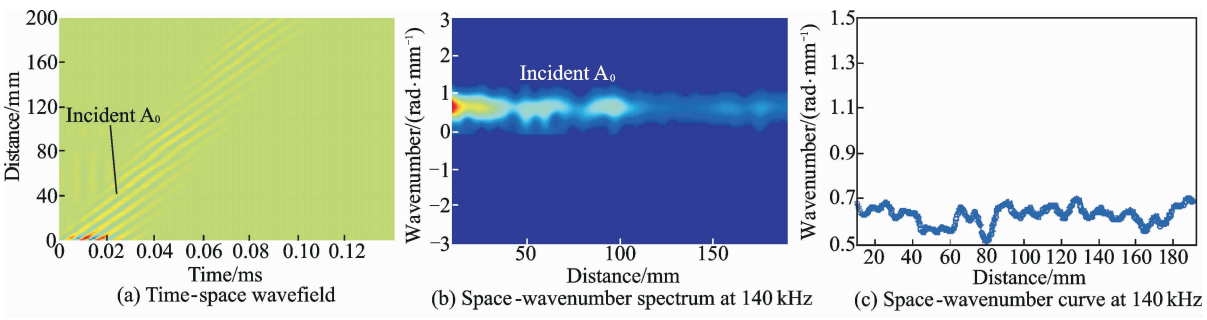

Fig. 13 Space-frequency-wavenumber analysis of experimental data for No. 1 plate by using laser-laser method

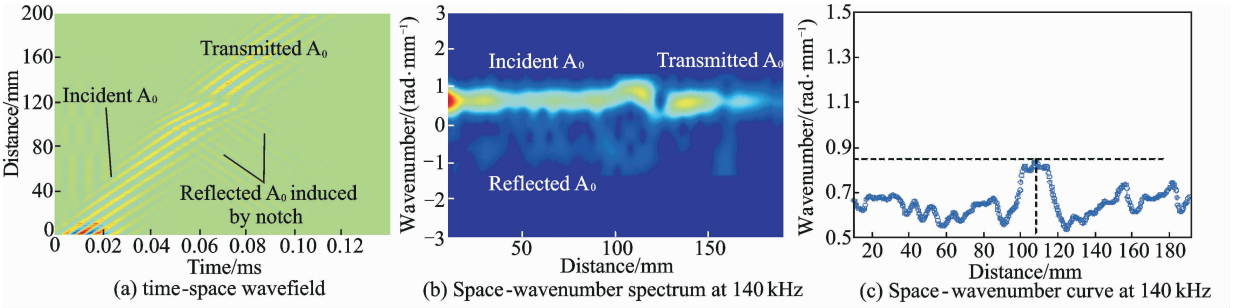

Fig. 14 Space-frequency-wavenumber analysis of experimental data for No. 2 plate by using laser-laser method

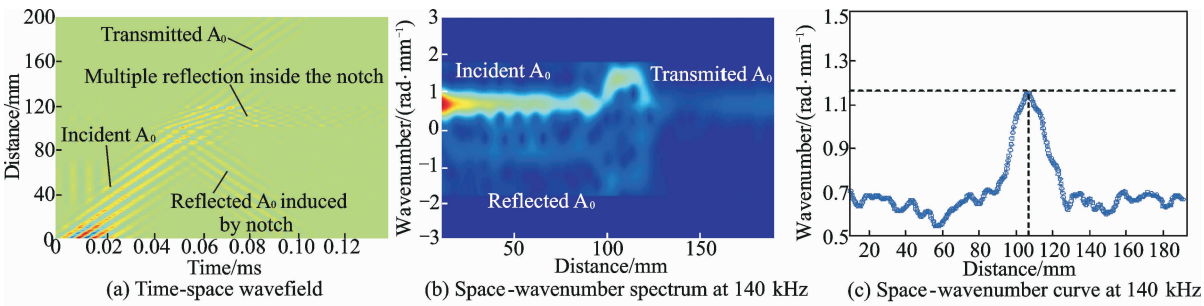

Fig. 15 Space-frequency-wavenumber analysis of experimental data for No. 3 plate by using laser-laser method

4 Conclusions

In this paper, the quantitative detection of notch defects in aluminium plates has been carried out by means of wavenumber analysis. Firstly, the simulated signals were analyzed to obtain the effects of notch depth, notch width and window width on the quantitative detection accuracy of wavenumber analysis. The results show that in order to minimize error in wavenumber measurement, the window width must be at least as large as two wavelengths and the notch must be at least as large as the window width. This implies that higher frequency excitations should perform better due to shorter wavelength and therefore smaller available window width and more accurate characterization of small defects. Laser-laser method was used in experimental investigation for signal excitation and reception. The simulation results showed that as the notch depth increase, the notch depth evaluation error decreases. However, in the experimental results, the detection error of notch with 1.4 mm depth increased. The poor consistency of experimental signals and Gaussian white noise in experimental data may be responsible for this phenomenon. We only briefly illustrate some factors that influence the detection accuracy of detecting the existance of some wavenumber, and have not considered other factors. The simulation and experimental results verify the feasibility of the wavenumber analysis method on evaluating the depth of the rectangular notch, which implies the method's potential in the quantitative detection of defects.

Acknowledgements

This work was supported by the National Natural Science Foundation of China (Nos. 51475012, 11772014, and 11272021).

References:

[1] WILCOX P D, LOWE M J S, CAWLEY P. The effect of dispersion on long-range inspection using ultrasonic guided waves [J]. NDT&E International, 2001, 34(1): 1-9.

[2] PRADO V T, HIGUTI R T, KITANO C, et al. Lamb mode diversity imaging for non-destructive testing of plate-like structures [J]. NDT&E International, 2013, 59: 86-95.

[3] LIU Z H, SUN K M, SONG G R, et al. Damage localization in aluminum plate with compact rectangular phased piezoelectric transducer array [J]. Mechanical Systems and Signal Processing, 2016, 70: 625-636.

[4] AN Y K, PARK B, SOHN H. Complete noncontact laser ultrasonic imaging for automated crack visualization in a plate [J]. Smart Materials and Structures, 2013, 22(2): 025022.

[5] YU L Y, LECKEY C A C. Lamb wave-based quantitative crack detection using a focusing array algorithm [J]. Journal of Intelligent Material Systems and Structures, 2013, 24(9): 1138-1152.

[6] LEE J R, JEONG H, CHIA C C, et al. Application of ultrasonic wave propagation imaging method to automatic damage visualization of nuclear power plant pipeline [J]. Nuclear Engineering and Design, 2010, 240(10): 3513-3520.

[7] LEE J R, CHIA C C, PARK C Y, et al. Laser ultrasonic anomalous wave propagation imaging method with adjacent wave subtraction: algorithm [J]. Optics and Laser Technology, 2012, 44(5): 1507-1515.

[8] MICHAELS J, DAWSON A, MICHAELS T, et al. Approaches to hybrid SHM and NDE of composite aerospace structures [C]// Proceedings of SPIE—The International Society for Optical Engineering. [S. l]; [s. n.], 2014, 9064:906427.

[9] TIAN Z H, YU L Y, LECKEY C A C. Rapid guided wave delamination detection and quantification in composites using global-local sensing [J]. Smart Materials and Structures, 2016, 25(8): 1-11.

[10] ALLEYNE D N, CAWLEY P. A two-dimensional Fourier transform method for the measurement of propagating multimode signals [J]. Journal of the Acoustical Society of America, 1991, 89(3): 1159-1168.

[11] YU L Y, TIAN Z H. Lamb wave structural health monitoring using a hybrid PZT-laser vibrometer approach [J]. Structural Health Monitoring, 2013, 12 (5-6): 469-483.

[12] RUZZENE M. Frequency-wavenumber domain filtering for improved damage visualization [J]. Smart Materials and Structures, 2007, 16(6): 2116-2129.

[13] KUDELA P, RADZIENSKI M, OSTACHOWICZ W. Identification of cracks in thin-walled structures by means of wavenumber filtering [J]. Mechanical Systems and Signal Processing, 2015, 50: 456-466.

[14] SOHN H, DUTTA D, YANG J, et al. Automated detection of delamination and disbond from wavefield images obtained using a scanning laser vibrometer [J]. Smart Materials and Structures, 2011, 20(4): 045017.

[15] FLYNN E B, CHONG S Y, JARMER G J, et al. Structural imaging through local wavenumber estimation of guided waves [J]. NDT&E International, 2013, 59: 1-10.

[16] ROGGE M D, LECKEY C A C. Characterization of impact damage in composite laminates using guided wavefield imaging and local wavenumber domain analysis [J]. Ultrasonics, 2013, 53: 1217-1226.

[17] MCAULAY R J, QUATIERI T F. Speech analysis/synthesis based on sinusoidal representation [J]. IEEE Transactions on Acoustics, Speech, and Signal Processing. 1986, 34(4): 744-754.

[18] LI F C, MENG G, KAGEYAMA K, et al. Optimal mother wavelet selection for Lamb wave analyses[J]. Journal of Intelligent Material Systems and Structures, 2009, 20(10): 1147-1161.

[19] MALINOWSKI P, WANDOWSKI T, KUDELA P, et al. Laser vibrometry for guided wave propagation phenomena visualisation and damage detection [C]// AIP Conference Proceedings. [S. l.]:[s. n.], 2010, 1253:140-149.

Prof. **Liu Zenghua** received his Ph. D. degree in mechanical engineering from Beijing University of Technology in 2006. Now, he is a professor and doctoral supervisor in Beijing University of Technology. His main research interests include ultrasonic nondestructive testing, structural health monitoring and modern measurement and control technology.

Mr. **Feng Xuejian** received his B. S. degree in Measurement and Control Technology and Instrumentation from Inner Mongolia University of Technology in 2015. Now, he is a postgraduate in Beijing University of Technology. His main research interests include laser ultrasonic nondestructive testing and wavefiled analysis technology.

Prof. **He Cunfu** received his B. S. degree from Taiyuan University of Technology in 1985, his M. S. degree from Huazhong University of Science and Technology in 1990, and his Ph. D. degree from Tsinghua University in 1996. He is a professor and doctoral supervisor in Beijing University of Technology. His main research interests include measurement theory, new ultrasonic nondestructive testing technologies, and sensors and measurement technology.

Prof. **Wu Bin** received his B. S. degree from Tianjin University in 1984, his M. S. degree from Beihang University in 1990 and his Ph. D. degree from Taiyuan University of Technology in 1996. Now, he is a professor and doctoral supervisor in Beijing University of Technology. His main research interests include experimental solid mechanics, modern measurement and control technology.

(Production Editor: Zhang Bei)